Effect of Temperature on the Capacitance of Carbon Nanotube Supercapacitors

Charan Masarapu, Hai Feng Zeng, Kai Hsuan Hung, and Bingqing Wei*

Department of Mechanical Engineering, University of Delaware, Newark, Delaware 19716

ARTICLE

ABSTRACT The effect of temperature on the kinetics and the diffusion mechanism of the ions in a supercapacitor assembled with single-walled carbon nanotube (SWNT) film electrodes and an organic electrolyte were thoroughly investigated. An improved room temperature performance of the supercapacitor was observed due to the combined effects of an increase in the conductivity of the SWNT films and surface modifications on the SWNT films by repeatedly heating and cooling the supercapacitor between the temperatures of 25 and 100 °C. Modified Randles equivalent circuit was employed to carry out an extensive analysis of the Nyquist spectra measured at different temperatures between 25 and 100 °C in order to understand the fundamentals of the capacitive and resistive variations in the supercapacitor. The experimental results and their thorough analysis will have significant impact not only on the fundamental understanding of the temperature-dependent electrode/electrolyte interfacial properties but also on supercapacitor design with appropriate electrode materials for numerous industrial and consumer applications. The supercapacitor with SWNT film electrodes was capable of withstanding current densities as high as 100 A/g, yielding eminent specific power density values of about 55 kW/kg. Ultralong galvanostatic charge—discharge cycling over 200 000 cycles with a constant current density of 20 A/g at 25 and 100 °C, respectively, showed excellent stability in capacitance with more than 80% efficiency. The usage of such a supercapacitor potentially enables far-reaching advances in backup energy storage and high pulse power applications.

KEYWORDS: single-walled carbon nanotube · temperature effect · supercapacitor · impedance spectroscopy · ionic diffusion

Supercapacitors are becoming attractive power sources in memory backup devices, electric vehicles, military weapons, space equipment, and in a number of day-to-day electronic equipment.[1−4] Especially for military, space, and electric vehicle applications, supercapacitors with high energy and power densities that can withstand harsh temperature environments are extremely desirable. To design a supercapacitor for a specific application that requires high energy density or high power density or both, proper electrode materials and a suitable electrolyte are to be chosen. For this purpose, it is of utmost importance to have the fundamental understanding of the interface properties of the electrode/electrolyte, such as the interface structure, charge transfer, ion diffusion, *etc.*, which play a vital role in governing the rate capability and specific capacitance of the supercapacitor. Cyclic voltammetry (CV) and electrochemical impedance spectroscopy (EIS) are some of the powerful characterization techniques that have the capability to throw light on such electrode/electrolyte properties in a supercapacitor assembly.

Carbon, in its various forms, is currently the most extensively examined and widely utilized electrode material in supercapacitors.[5−7] While extensive work has been done in understanding the kinetics and diffusion mechanism of ions in the activated carbons[8,9] and in nanosized carbon materials[10,11] at room temperature, very little research has been realized on the temperature-dependent studies. Organic electrolytes in general have wide voltage windows of operation and high decomposition temperatures, compared to aqueous electrolytes.[12−15] Until recently, the temperature-dependent studies on supercapacitors assembled with conventional carbonaceous materials in an organic electrolyte have been limited to around 70 °C.[16,17] However, these studies did not address the effects of rigorous temperature conditions such as the repeated heating and cooling, continuous high temperature, *etc.* on the supercapacitor performance, which are practically important for commercial applications. Moreover, there has been no systematic work on the temperature effects on the nanosized carbon electrodes in supercapacitors compared with the conventional carbonaceous materials.

Carbon nanotubes (CNTs), with their unique architecture,[18] excellent conductivity,[19] and high surface area[20] have drawn significant attraction as nanosized supercapacitor electrodes.[21,22] Rate capability

*Address correspondence to weib@udel.edu.

Received for review May 14, 2009 and accepted July 01, 2009.

Published online July 7, 2009.
10.1021/nn900500n CCC: $40.75

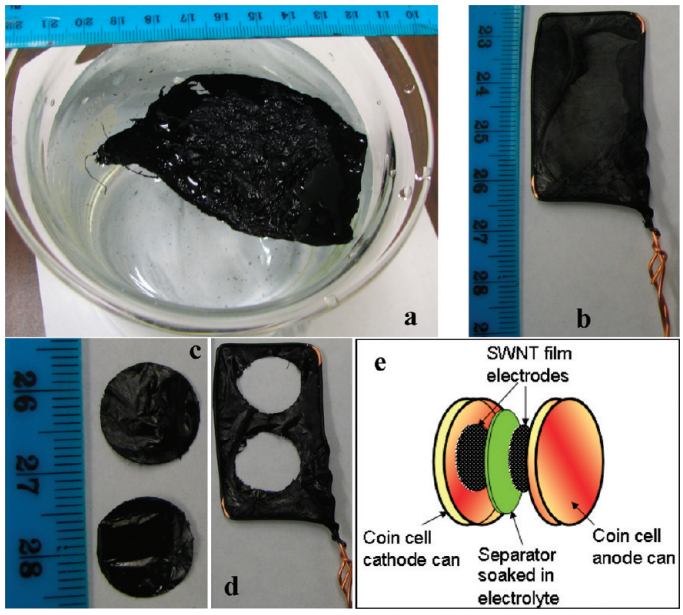

Figure 1. Photographs illustrating the free-standing SWNT electrode preparation process. (a) Purified SWNT film on water surface. (b) Free-standing SWNT film on the wire loop. (c) Electrodes with 1.25 cm diameter punched from the free-standing SWNT film. (d) SWNT film on the wire loop after punching the electrodes. (e) Schematic representation of the supercapacitor coin cell assembly with the free-standing SWNT films without any current collectors. A Teflon O-ring was used to seal the coin cell to perform high-temperature measurements up to 100 °C.

studies determine the rate at which the supercapacitor can be charged and discharged. Extremely high rate capabilities can be achieved by utilizing CNT electrodes in supercapacitors when compared to the conventional carbonaceous materials.[23,24] Especially the single-walled carbon nanotubes (SWNTs) can be synthesized as long tube structures[25] that are favorable for preparing entangled mats of free-standing electrodes with the filtration technique.[26] The free-standing films can be used directly as electrode materials without any complex nanotube coating procedures,[27] and there is no requirement for the current collector. The supercapacitors assembled with such free-standing SWNT films have shown good capacitance stability and high rate capability and yielded reasonable specific capacitance values at room temperature in both aqueous and organic electrolytes.[28−31]

Here, we report the temperature effects of a coin cell supercapacitor assembled with free-standing SWNT film electrodes and tetraethylammonium tetrafluoroborate−polypropylene carbonate ($TEABF_4$/PC) electrolyte under rigorous temperature conditions (25−100 °C). Unlike the filtration technique, where the nanotubes are dispersed in a solution and filtered to obtain the free-standing SWNT films,[26] we utilized the SWNT films directly synthesized by a chemical vapor deposition (CVD) method reported elsewhere[32] with post-purification techniques that did not involve a complex filtration process to prepare the electrodes. Electrochemical characterization techniques, cyclic voltammetry, and the electrochemical impedance spectroscopy were used to extensively analyze the electrode/electrolyte interface properties in the supercapacitor with respect to changes in the temperature. Effects of repeated heating and cooling on the performance of the supercapacitor was studied and compared to the results of the supercapacitor with activated carbon fabric.[33] In addition, ultralong cycle galvanostatic charge−discharge has been carried out at temperatures 25 and 100 °C with repeated heating and cooling to demonstrate the long-term stability of the supercapacitor with the SWNT film electrodes.

RESULTS AND DISCUSSION

Figure 1 shows the electrode preparation from the free-standing SWNT films and the schematics of a supercapacitor cell assembly (detailed information can be found in the Methods section). The cyclic voltammograms (CVs) of the cell were measured in the voltage window of −1.5 to +1.5 V (actual potential of operation is 1.5 V) with scan rates of 50, 100, 200, 500, and 1000 mV/s at each set of temperatures, 25, 50, 75, and 100 °C (Supporting Information, Figure S1). Figure 2a,b displays the CVs measured at 50 and 1000 mV/s at 25, 100, and 25 °C after cooling back from 100 °C. The voltammograms were close to rectangular shape at 50 mV/s as well as at a very high scan rate of 1000 mV/s, indicating ideal capacitive behavior within this wide temperature window. Figure 2c shows the capacitance values of the cell calculated from the voltammograms (Supporting Information S1) measured at different temperatures and plotted with respect to the scan rate.

Interesting results can be observed from these figures. An increasing pseudocapacitive behavior in the voltammograms was observed with the increase in the temperature from 25 to 100 °C, similar to perfectly reversible Faradaic reactions taking place in the capacitor. Generally, the Faradaic process involves the electron transfer across the double layers with a consequent change of oxidation state, and the measurable capacitance arising due to this process is designated as a pseudocapacitance. In Figure 2a,b, the pseudocapacitive behavior is indicated by the ovals. The capacitance at all scan rates gradually increased with the increase in temperature (Figure 2c). Figure 2c also illustrates the performance of the cell with repeated heating and cooling. The value of the capacitance at all scan rates obtained at 25 °C after cooling back from 100 °C has a slight increase (about 10%) compared to the capacitance values obtained initially at the same temperature of 25 °C. In the present experiment, the maximum potential was limited to 1.5 V during the CV measurements, but as the cell is being heated, even though the potential is within the safe decomposition limit of the PC electrolyte,[12] some electrolyte will evaporate and increases the vapor pressure inside the cell. The trace amount of evolved gases from the electrolyte system[34,35] modifies the surface of the SWNT electrode,

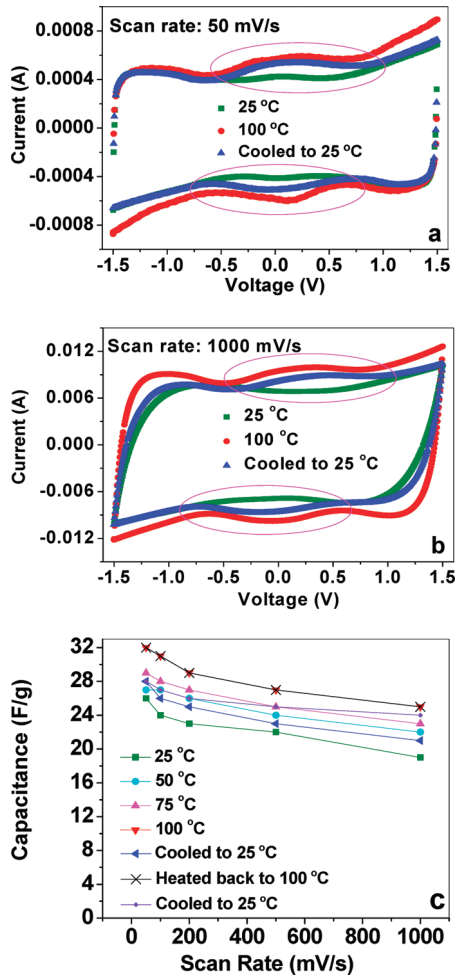

Figure 2. Cyclic voltammograms of the cell at different temperatures with various scan rates: (a) 50 and (b) 1000 mV/s. The ovals represent pseudocapacitive behavior in the voltammograms with perfectly reversible Faradaic reactions taking place in the capacitor. The pseudocapacitive behavior is present in the CVs at 25 °C even after cooling from 100 °C. (c) Capacitance of the cell calculated from CVs at different scan rates and at different temperatures *versus* the scan rate. Also illustrated is the capacitance of the cell with repeated heating and cooling between 25 and 100 °C. Due to the introduction of Faradaic reactions, an increase in the capacitance is observed at high temperature.

which possibly leads to the physisorbtion of the electrolyte ions at high temperature, giving rise to the Faradaic currents in the CVs (Figure 2a,b) and causing an increase in the capacitance when heated from 25 to 100 °C (Figure 2c). The surface modification of the SWNT films is partially irreversible, and the physisorbtion remains even at 25 °C (refer to the ovals in Figure 2a,b) after cooling from 100 °C. This is evidenced by the CV curve which shows the pseudocapacitive behavior with a capacitance value obtained at 25 °C, slightly higher than the previously obtained value at the same temperature of 25 °C (Figure 2c). The effects of this phenomenon on the values of the capacitance can be further explained in detail by the electrochemical impedance spectroscopy (EIS) measurements presented in the subsequent paragraphs.

The principle objective of the EIS measurements is to gain insight into the temperature dependence of the resistive and capacitive elements and their effects on the performance of the supercapacitor. Figure 3a shows the Nyquist spectra in the frequency range of 100 kHz to 10 mHz measured at equilibrium open circuit potential (~0 V) at different temperatures from 25 to 100 °C with repeated heating and cooling. The Nyquist spectrum can be represented by a modified Randles circuit[36] with a set of resistors and capacitors in series and parallel as shown in Figure 3b. The first intersection point on the real axis of the Nyquist spectrum in the high-frequency region provides the value of the ohmic resistance of the electrolyte and the internal resistance of the electrode materials and is represented as R_S. The semicircle in the high-frequency region to midfrequency is modeled by an interfacial charge transfer resistance R_{CT} and the double layer capacitance C_{DL} connected parallel to each other. After the semicircle, the Nyquist spectrum shows a long tail in the low-frequency region pertaining to the diffusion of ions into the bulk of the electrode. The transition from the high-frequency semicircle to the midfrequency tail is represented by the Warburg element W_o, which is expressed as $A/(j\omega)^n$, where A is called the Warburg coefficient, ω is the angular frequency, and n is an exponent. At very low frequencies, an ideally polarizable capacitance would give rise to a straight line parallel to the imaginary axis with a mass capacitance represented as C_L. However, from Figure 3a, it can be observed that the spectra obtained at low-frequency range (~1 Hz to 10 mHz) are inclined at an angle to the real impedance axis, suggesting that a resistive element is associated with C_L. This resistance can be designated as the low-frequency leakage resistance R_{leak} and is placed parallel to C_L in the equivalent circuit. Figure 3c shows the Nyquist spectra measured at different temperatures plotted on a shifted real axis emphasizing the high-frequency semicircle and the midfrequency spike (100 kHz to 1 Hz).

To obtain all of the equivalent circuit parameters, the fitting of the impedance expression obtained from the equivalent circuit to the experimental Nyquist spectra in the whole frequency range from 100 kHz to 10 mHz was performed using the EIS data fitting program ZVIEW. All of the fitting parameters of the Nyquist spectra at all temperatures are shown in the table format in Figure 3d. The value of R_S is significantly decreased with the increase in the temperature from 25 to 100 °C. The decrease is caused by an increase in the conductivity of the electrolyte due to the enhanced mobility of the ions in the electrolyte with the increase in the temperature but is not contributed by the intrinsic temperature dependence of the SWNTs themselves. This is verified by measuring the variation in the resistance of the SWNT film from 25 to 100 °C without the involvement of the electrolyte. Similar to the SWNT bundles,

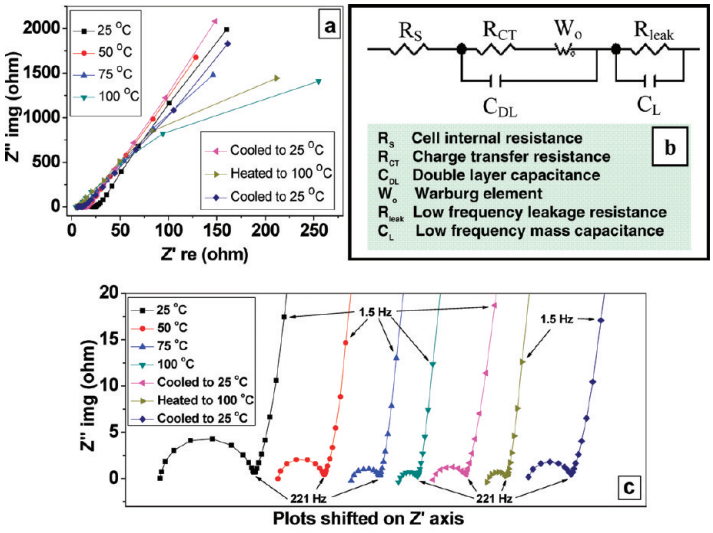

D Fitting parameters		25 °C	50 °C	75 °C	100 °C	Cooled to 25 °C	Heated to 100 °C	Cooled to 25 °C
R_S (Ω)		14.0	10.8	9.9	4.8	10.4	5.1	6.4
R_{CT} (Ω)		9.1	4.4	2.5	1.6	2.9	1.6	2.9
C_{DL} (μF)		3	8	16	28	13	27	12
$W_o = A/(j\omega)^n$	A (Ω.s^{-n})	173	166	170	106	250	130	240
	n	0.60	0.63	0.66	0.66	0.64	0.66	0.64
R_{leak} (k Ω)		38.66	30.82	18.92	8.90	41.33	11.00	30.00
$C_L \sim 2/\omega Z''$ (F/g)		23.4	27.94	31.71	32.57	22.74	31.71	25.00

Figure 3. Electrochemical impedance spectroscopy measurements on the supercapacitor at different temperatures with repeated heating and cooling. (a) In the frequency range from 100 kHz to 10 mHz. (b) Randles equivalent circuit representing the circuit elements in the Nyquist spectra. The equivalent circuit is used to fit the Nyquist spectra using the software ZVIEW. (c) High-frequency response of the Nyquist spectra of panel a showing the semicircles plotted on the shifted real axis for clarity. (d) Equivalent circuit parameters obtained from the fitting results. The performance of the cell when cooled back to 25 °C improved due to betterment of R_S, R_{CT}, C_{DL}, and W_o values compared to the as-assembled cell at 25 °C.

which act as metallic conductors at ambient temperatures,[37] the resistance of the SWNT film increased by about 8% at 100 °C compared to the value at 25 °C (conductivity is about 0.2 S/cm at 25 °C).

The physisorbtion of the electrolyte ions on the SWNT electrodes with the increase in the temperature can be explained based on the variations in the values of C_{DL} and R_{CT}. At high frequencies, the double layer capacitance C_{DL} arises from the charges present close to the surface of the SWNT film that overcome the energy to migrate with the alternating potential. The surface modification of the SWNTs by the evolved gases from the electrolyte presumably provides more accessible sites for the mobile charges near the surface of the SWNT electrode thus leading to an increase in the value of C_{DL} from 3 μF at 25 °C to 28 μF at 100 °C. Also, the value of the C_{DL} obtained at 25 °C after cooling from 100 °C is higher than the value obtained at 25 °C before heating. So it should be obvious that the physisorbtion is taking place even at 25 °C after cooling back from 100 °C. R_{CT} actually represents the resistance of the charges in the pores of the SWNT electrode. A reduction in the value of R_{CT} implies that the surface modification is also increasing the conductivity of the SWNT films. This is evident from the lower values of the R_{CT} at 25 °C after cooling from 100 °C, compared to the values obtained at 25 °C before heating from the fitting parameters in Figure 3d.

Some of the important features of the CVs in Figure 2 can also be explained based on the fitting parameters in Figure 3d. Generally, the Warburg element represents the diffusion of ions into the pores on the surface of the electrode during the transition from the high-frequency semicircle to the midfrequency spike. Porous electrodes such as activated carbons generate an exponent value of $n = 0.5$, where the spike is at an angle of 45° to the real axis at room temperature.[38] For the case of SWNTs in this study, it can be observed that the value of n is 0.6 at 25 °C with the spike near vertical to the real impedance axis yielding an ideal capacitive behavior. The higher value of the exponent indicates that the ion diffusion is taking place only on the surface of the SWNT electrode and suggests that the SWNTs are not behaving as typical porous electrodes,[33] which is evident from the BET surface area measurements on the SWNT films (see Supporting Information S3 and Figure S2). Also, the transition from the high-frequency semicircle to the midfrequency spike as shown in Figure 3c is occurring at relatively higher frequency of ~221 Hz in the case of SWNTs compared to porous carbon electrodes.[23,33] The high rate capability of the SWNT film supercapacitor compared to the porous electrodes is the direct consequence of the surface diffusion effects with high exponent values in the Warburg element and a higher transition frequency from the semicircle to the vertical spike. Therefore, the CVs do not deviate much from the rectangular shape even at a scan rate as high as 1000 mV/s in the case of the supercapacitor with carbon nanotube electrodes. Even though the rate capability is high for carbon nanotube electrodes, the nonporous nature and the surface diffusion effects limit the number of ions that form the double layer at the electrode surface and yield lower gravimetric capacitance compared to the capacitor employing an activated carbon material.[33]

With an increase in the temperature from 25 to 100 °C, the value of n is increasing and the Warburg coefficient A is decreasing. This leads to a better rate capability of the supercapacitor at high temperature and is evident from the loop obtained at 100 °C, which is more rectangular than the loop obtained at 25 °C with a scan rate of 1000 mV/s in Figure 2b. However, it is interesting to note from the impedance data of Figure 3c that the variation of temperature does not lead to any shift in the frequency of the transition from the high-frequency semicircle to the midfrequency spike which is occurring at ~221 Hz. This behavior suggests that there is no time dependence in the charging process on temperature variation, and the physisorbtion of the electrolyte ions on the surface of the SWNT films at high

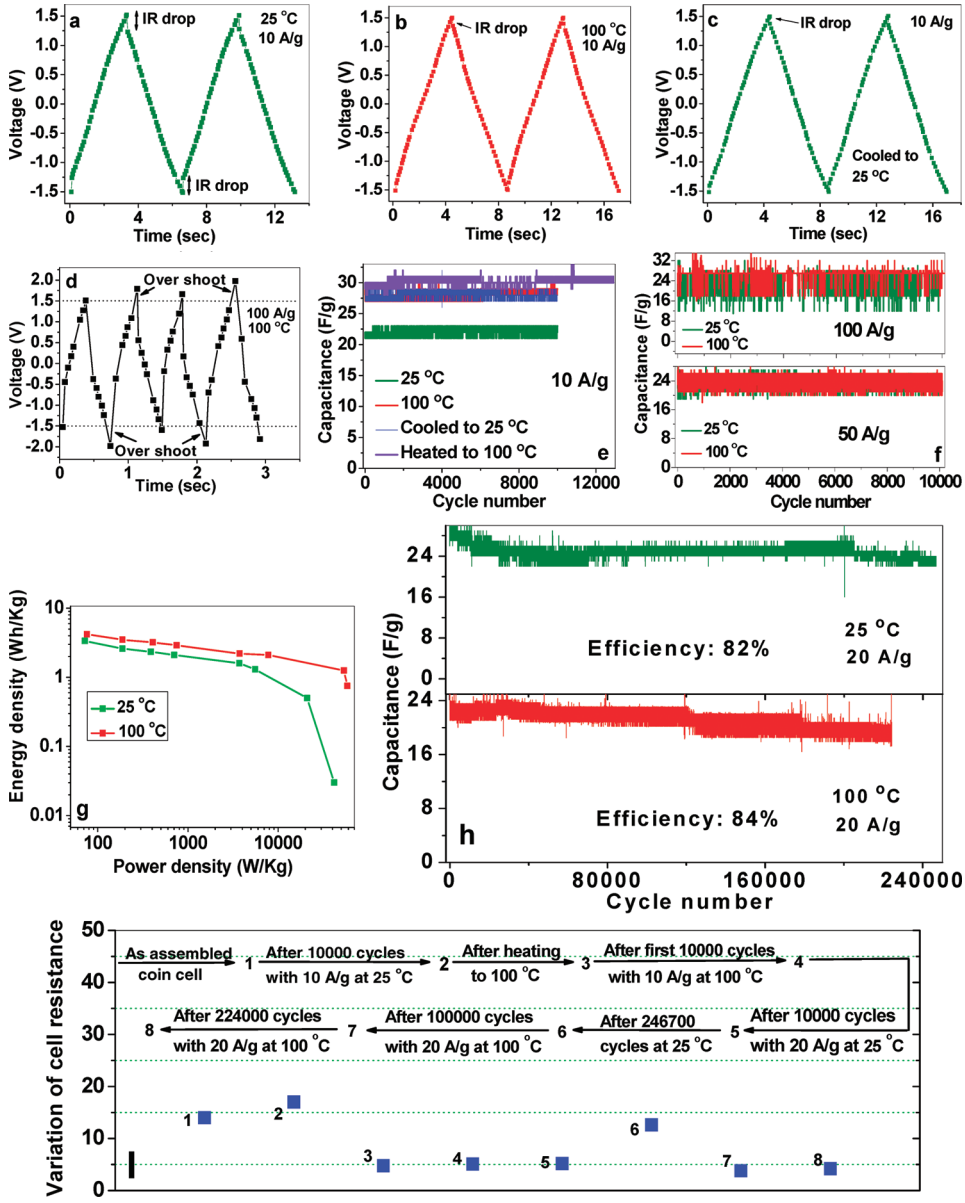

Figure 4. Long cycle galvanostatic charge−discharge studies on the supercapacitor measured at 25 and 100 °C with different current densities from 10 to 100 A/g. Charge−discharge curve obtained with a constant current density of 10 A/g at (a) 25, (b) 100, and (c) 25 °C after cooling from 100 °C. (d) Charge−discharge curve obtained with a constant current density of 100 A/g at 100 °C. (e) Long cycle discharge capacitance with a constant current density of 10 A/g at 25 and 100 °C with repeated heating and cooling. (f) Long cycle discharge capacitance with current densities of 50 and 100 A/g measured at 25 and 100 °C. (g) Ragone chart of the supercapacitor obtained from the discharge curves measured at different constant current densities at 25 and 100 °C. (h) Displaying the ultralong cycling stability of the cell by running 246 700 and 224 000 cycles of charge−discharge with a current density of 20 A/g at 25 and 100 °C. (i) Cell resistance variations in the coin cell at different stages of the charge−discharge measurements.

temperature (Figure 2) is happening at a fast rate without affecting the rate capability. From Figure 3d, the parameters are getting better at 25 °C with repeated heating and cooling thus leading to an improved performance at 25 °C after cooling from 100 °C compared to the performance of the as-assembled supercapacitor at 25 °C.

At very low frequency, the mass capacitances estimated from the fitting parameters in Figure 3d are comparable to the values obtained from CVs measured at the scan rate of 50 mV/s (Figure 2c) showing the validity of the fitting parameters. The low-frequency leakage resistance of the cell is decreasing from 38 kΩ at initial 25 °C to about 8 kΩ at 100 °C. Lower leakage resistance implies a higher leakage current that causes the cell to self-discharge faster.[16] Considering the variation of the overall parameters in Figure 3d, the performance of the supercapacitor coin cell with SWNT electrodes at 25 °C is improving with repeated heating and cooling. Such kind of improvement in the performance was not observed in case of the supercapacitor with activated carbon fabric electrodes.[33]

The improvement in the supercapacitor performance with SWNTs with repeated heating and cooling is further elucidated by the constant current charge−discharge cycling on the supercapacitor (see Supporting Information S4 for a sequence of charge−discharge measurements). Figure 4a−c shows typical charge−discharge curves of the supercapacitor at initial 25 °C, when heated to 100 °C and after cooling back to 25 °C, respectively, run at a constant current density of 10 A/g. A significant reduction in the IR drop can be observed in the charge−discharge curve obtained at 25 °C after cooling from 100 °C compared to the IR drop in the curve of the as-assembled sample at 25 °C.

To demonstrate the long-term stability of the supercapacitor, several tens of thousands of charge−discharge cycles were run at different constant current densities from 100 mA/g (81.46 mA/cm^2) to 100 A/g (81.46 A/cm^2) at 25 and 100 °C by repeated heating and cooling (see Supporting Information S4 for a sequence of charge−discharge measurements and Figure S3 for some charge−discharge measurements at 100 mA/g and 1 A/g). Figure 4d shows the charge− discharge curves of the supercapacitor at 100 °C, measured with constant current density of 100 A/g. The long cycle discharge capacitances of the cell calculated from the galvanostatic charge−discharge curves are displayed in Figure 4e,f. An impressive result of the supercapacitor is obvious from these measurements. The charge−discharge curves represented ideal capacitive behavior even at a current density as high as 100 A/g. As the current density was very high, large overshoots were observed in the charge−discharge curves over 1.5 V. Since the upper potential of operation for the $TEABF_4$/PC electrolyte system can be as high as 2.5 V,[12] the overshoots did not cause any negative effects such as electrolyte decomposition or cell failure. This is obvious from the long cycle performance tested by running over 10 000 charge−discharge cycles at 25 and 100 °C both at 50 and 100 A/g (Figure 4f). The slight changes in the slope of the charge−discharge curves lead to variations in the calculated capacitances (Supporting Information S5) at high current densities as shown in the Figure 4e,f (for example, $\sim 23 \pm 6$ F/g at 100 A/g).

Figure 4g shows the plot of specific energy density *versus* specific power density, also called a Ragone plot,[39] for the supercapacitor at 25 and 100 °C, respectively. The total weight of the two SWNT film electrodes was considered in estimating the energy and power density (Supporting Information S5). The supercapacitor has a maximum power density of about 55 kW/kg at 100 °C obtained with the discharge curve run at a constant current density of 100 A/g. The maximum energy density obtained from the discharge curve run with 100 mA/g at 100 °C is 4.2 Wh/kg. To obtain an optimum energy and power density for different applications, the cell can be operated with a large current density tolerance in the temperature range from 25 to 100 °C.

After all the long cycle measurements at different current densities with repeated heating and cooling, the cell was run at 25 °C for 246 700 and at 100 °C for additional 224 000 charge−discharge cycles with a constant current density of 20 A/g. Figure 4h shows the discharge capacitance of all the cycles at both temperatures. The cell showed excellent ultralong cycle stability at both 25 and 100 °C with an efficiency of approximately 82 and 84%, respectively. The efficiency was calculated based on the degradation in the value of discharge capacitance after all the charge−discharge cycles (246 700 cycles at 25 °C and 224 000 cycles at 100 °C) from the initial discharge capacitance obtained from the first charge−discharge cycle.

Since supercapacitors are power devices, the most important figure of merit to be considered is the stability of their impedance during the charge−discharge cycling with the repeated heating and cooling. Figure 4i shows the resistance R_S of the supercapacitor cell obtained from the EIS measurements at different stages of the charge−discharge measurements (see Supporting Information S4 for the sequence of charge−discharge measurements carried on the coin cell). There is no significant increase in the impedance of the cell even after running several thousands of charge−discharge cycles at 100 °C, implying a stable power output from the supercapacitor. It took more than 3 months to perform all of the charge−discharge measurements with repeated heating and cooling on the coin cell, and the cell is still operational. Figure 4 provides strong evidence that the supercapacitor with the free-standing SWNT film electrodes in $TEABF_4$/PC electrolyte can be conveniently operated at any current density from 100 mA/g to 100 A/g in the temperature range from 25 to 100 °C with no significant cell damage.

There are several advantages of utilizing the free-standing SWNT film synthesized from our method[32] as the supercapacitor electrodes. The foremost is that the SWNT can be handled as an entire film during the whole process of the synthesis, purification, and electrode preparation, which is extremely simple compared to the filtration technique.[26] The process can be easily expanded to acquire SWNT film electrodes with uniform thickness and on a large scale. The complex mixing and coating procedure[27] involved with the powder samples is not required. The SWNT film itself acts as a good conductor, thus eliminating the usage of the current collectors. By using the supercapacitors with the SWNT film electrodes and the $TEABF_4$/PC electrolyte, we demonstrated that the operating temperature can be easily expanded to 100 °C with extremely high rate capability.

CONCLUSIONS

In conclusion, the electrochemical performance of the coin cell supercapacitor assembled with SWNT film

electrodes using 1 M $TEABF_4$/PC electrolyte was systematically studied in a temperature window ranging from 25 to 100 °C. A pseudocapacitive behavior was observed in the cyclic voltammograms at high temperature, which was attributed to the physisorbtion of the electrolyte ions on the surface of the SWNTs. Fitting parameters of Nyquist spectra obtained from a modified Randles equivalent circuit revealed that repeated heating and cooling between 25 to 100 °C enhanced the room temperature performance of the supercapacitor. The long cycle galvanostatic charge−discharge measurements showed excellent stability in capacitance at both 25 and 100 °C, even at high current densities of 50 and 100 A/g. The stability of the cell was also reflected under rigorous temperature conditions and the super long galvanostatic charge−discharge cycles. The usage of such a supercapacitor potentially enables far-reaching advances in civilian, military, and aerospace applications.

METHODS

Fabrication of the SWNT Macrofilm Electrodes. The SWNT films were directly deposited on a copper foil by CVD method[28] using ferrocene as carbon feedstock/catalyst and sulfur as an additive to promote SWNT growth to a high percentage. There is no additional carbon source (*e.g.*, xylene, hexane, and methane) required for the synthesis. The deposited films were peeled off from the copper foil and were purified by first heating in air up to 450 °C for 1 h to remove amorphous carbon and then treated in 9 M HCl solution for 0.5 h to remove the iron catalyst particles. After the acid treatment, the film was thoroughly washed with DI water. The purification process did not involve any filtration technique, and the SWNTs were handled as an entire film through the entire purification process. The complex entanglement of the long SWNT strands provided strong mechanical stability for the film. Figure 1a shows a purified SWNT film floating on the water surface. The film was transferred directly from the beaker onto a wire mesh (loop), as shown in Figure 1b. After drying the film, two 1.25 cm diameter electrodes were punched with an arch punch. The photographs of the punched electrodes and the wire mesh after the electrodes were punched can be seen from Figure 1c,d. The thickness as well as the weight of the electrodes can be controlled by varying the number of layers of the SWNT films deposited on the wire mesh.

Supercapacitor Assembly. The supercapacitor was assembled in a 2032 coin cell with a pair of SWNT films weighing 0.7 mg each, without any current collectors. A 1 M $TEABF_4$ (Alfa Aesar) dissolved in battery-graded PC (Alfa Aesar) solvent was used as the electrolyte. A Wattman glass microfiber filter paper soaked in the electrolyte was used as the separator. The coin cell was sealed using a Teflon gasket to withstand temperatures up to 150 °C. The supercapacitor assembly was carried out in a glovebox (MBraun, Unilab) with oxygen and water vapor levels less than 0.1 ppm. For the temperature-dependent measurements from 25 up to 100 °C, the coin cell was placed in a box oven (LINBERG/BLUE M) capable of maintaining a very stable set temperature up to one-tenth of a °C. Figure 1e shows the experimental arrangement of the supercapacitor.

Electrochemical Measurements. The electrochemical characterization at different temperatures was done by measuring the cyclic voltammograms, electrochemical impedance spectra, and constant current charge−discharge curves. Cyclic voltammograms and the electrochemical impedance spectra of the supercapacitor were measured with an EG&G Parstat 2273 potentiostat/galvanostat. The galvanostatic charge−discharge examination was carried out by an Arbin battery testing system.

Acknowledgment. This work was financially supported by the National Science Foundation (NSF CMMI #0753462) and the Delaware NASA EPSCoR Research Infrastructure Development (RID) Award.

Supporting Information Available: Cyclic voltammograms of the coin cell supercapacitor at different temperatures from 25 to 100 °C measured at different scan rates from 50 to 1000 mV/s. Surface area measurements on purified SWNT macrofilms. Sequence of charge−discharge measurements carried on the coin cell at different temperatures. Long cycle charge−discharge measurements at current densities of 100 mA/g and 1 A/g. This material is available free of charge *via* the Internet at http://pubs.acs.org.

REFERENCES AND NOTES

1. Miller, J. R.; Simon, P. Electrochemical Capacitors for Energy Management. *Science* **2008**, *321*, 651–652.
2. Burke, A. R&D Considerations for the Performance and Application of Electrochemical Capacitors. *Electrochim. Acta* **2007**, *53*, 1083–1091.
3. Conway, B. E.; Pell, W. G. Double-Layer and Pseudocapacitance Types of Electrochemical Capacitors and Their Applications to the Development of Hybird Devices. *J. Solid State Electrochem.* **2003**, *7*, 637–644.
4. Kotz, R.; Carlen, M. Principles and Applications of Electrochemical Capacitors. *Electrochim. Acta* **2000**, *45*, 2483–2498.
5. Simon, P.; Gogotsi, Y. Materials for Electrochemical Capacitors. *Nat. Mater.* **2008**, *7*, 845–854.
6. Chmiola, J.; Yushin, G.; Gogotsi, Y.; Portet, C.; Simon, P.; Taberna, P. L. Anomalous Increase in Carbon Capacitance at Pore Sizes Less than 1 Nanometer. *Science* **2006**, *313*, 1760–1763.
7. Frackowiak, E. Carbon Materials for Supercapacitor Application. *Phys. Chem. Chem. Phys.* **2007**, *9*, 1774–1785.
8. Frackowiak, E.; Beguin, F. Carbon Materials for the Electrochemical Storage of Energy in Capacitors. *Carbon* **2001**, *39*, 937.
9. Qu, D. Y. Studies of the Activated Carbons Used in Double-Layer Supercapacitors. *J. Power Sources* **2002**, *109*, 403–411.
10. Frackowiak, E.; Metenier, K.; Bertagna, V.; Beguin, F. Supercapacitor Electrodes from Multiwalled Carbon Nanotubes. *Appl. Phys. Lett.* **2000**, *77*, 2421–2423.
11. Liu, C. G.; Liu, M.; Li, F.; Cheng, H. M. Frequency Response Characteristic of Single-Walled Carbon Nanotubes as Supercapacitor Electrode Material. *Appl. Phys. Lett.* **2008**, *92*, 143108.
12. Ue, M.; Ida, K.; Mori, S. Electrochemical Properties of Organic Liquid Electrolytes Based on Quaternary Onium Salts for Electrical Double-Layer Capacitors. *J. Electrochem. Soc.* **1994**, *141*, 2989–2996.
13. Kurzweil, P.; Chwistek, M. Electrochemical Stability of Organic Electrolytes in Supercapacitors: Spectroscopy and Gas Analysis of Decomposition Products. *J. Power Sources* **2008**, *176*, 555–567.
14. Macneil, D. D.; Dahn, J. R. Can an Electrolyte for Lithium-Ion Batteries Be Too Stable. *J. Electrochem. Soc.* **2003**, *150*, A21–A28.
15. Li, X. H.; Meng, Y. Z.; Zhu, Q.; Tjong, S. C. Thermal Decomposition Characteristics of Poly(propylene carbonate) Using TG/IR and Py-GC/MS Techniques. *Polym. Degrad. Stab.* **2003**, *81*, 157–165.
16. Kotz, R.; Hahn, M.; Gallay, R. Temperature Behavior and Impedance Fundamentals of Supercapacitors. *J. Power Sources* **2006**, *154*, 550–555.
17. Liu, P.; Verbrugge, M.; Soukiazian, S. Influence of Temperature and Electrolyte on the Performance of

Activated-Carbon Supercapacitors. *J. Power Sources* **2006**, *156*, 712–718.
18. Wei, B. Q.; Vajtai, R.; Jung, Y.; Ward, J.; Zhang, R.; Ramanath, G.; Ajayan, P. M. Organized Assembly of Carbon Nanotubes. *Nature* **2002**, *416*, 495–496.
19. Wei, B. Q.; Vajtai, R.; Ajayan, P. M. Reliability and Current Carrying Capacity of Carbon Nanotubes. *Appl. Phys. Lett.* **2001**, *79*, 1172–1174.
20. Peigney, A; Laurent, Ch; Flahaut, E; Bacsa, R. R.; Rousset, A. Specific Surface Area of Carbon Nanotubes and Bundles of Carbon Nanotubes. *Carbon* **2001**, *39*, 507–514.
21. Niu, C; Sichel, E. K; Hoch, R; Moy, D.; Tennent, H. High Power Electrochemical Capacitors Based on Carbon Nanotube Electrodes. *Appl. Phys. Lett.* **1997**, *70*, 1480–1482.
22. Dalton, A. B.; Collins, S.; Munoz, E.; Razal, J. M.; Ebron, V. H.; Ferraris, J. P.; Coleman, J. N.; Kim, B. G.; Baughman, R. H. Super-Tough Carbon-Nanotube Fibres. *Nature* **2003**, *423*, 703.
23. Obreja, V. V. N. On the Performance of Supercapacitors with Electrodes Based on Carbon Nanotubes and Carbon Activated Material—A Review. *Physica E* **2008**, *40*, 2596–2605.
24. Futaba, D. N.; et al. Shape-Engineerable and Highly Densely Packed Single-Walled Carbon Nanotubes and Their Application as Super-Capacitor Electrodes. *Nature* **2006**, *5*, 987–994.
25. Zhu, H. W.; Xu, C. L.; Wu, D. H.; Wei, B. Q.; Vajtai, R.; Ajayan, P. M. Directly Synthesis of Long Nanotube Strands. *Science* **2002**, *296*, 884–886.
26. Baughman, R. H.; *et al.* Carbon Nanotube Actuators. *Science* **1999**, *284*, 1340–1344.
27. An, K. H.; Kim, W. S.; Park, Y. S.; Moon, J. M.; Bae, D. J.; Lim, S. C.; Lee, Y. S.; Lee, Y. H. Electrochemical Properties of High Power Supercapacitors Using Single-Walled Carbon Nanotube Electrodes. *Adv. Funct. Mater.* **2001**, *11*, 387–392.
28. Shiraishi, S.; Kurihara, H.; Okabe, K.; Hulicova, D.; Oya, A. Electrical Double Layer Capacitance of Highly Pure Single-Walled Carbon Nanotubes (hipco Buckytubes) in Propylene Carbonate Electrolytes. *Electrochem. Commun.* **2002**, *4*, 593–598.
29. Barisci, J. N.; Wallace, G. G.; Chattopadhyay, D.; Papadimitrakopoulos, F.; Baughman, R. H. Electrochemical Properties of Single-Wall Carbon Nanotube Electrodes. *J. Electrochem. Soc.* **2003**, *150*, E409–E415.
30. Frackowiak, E.; Jurewicz, K.; Delpeux, S.; Beguin, F. Nanotubular Materials for Supercapacitors. *J. Power Sources* **2001**, *97*, 822–825.
31. Barisci, J. N.; Wallace, G. G.; Baughman, R. H. Electrochemical Studies of Single-Wall Carbon Nanotubes in Aqueous Solutions. *J. Electroanal. Chem.* **2000**, *488*, 92–98.
32. Zhu, H. W.; Wei, B. Q. Direct Fabrication of Single-Walled Carbon Nanotube Macro-Films on Flexible Substrates. *Chem. Commun.* **2007**, *29*, 3042–3044.
33. Hung, K.; Masarapu, C. ; Tsehao, K.; Wei, B. Q. Wide-Temperature Range Operation Supercapacitors from Nanostructured Activated Carbon Fabric. *J. Power Sources* **2009**, *193*, 944–949.
34. Hahn, M.; Wursig, A.; Gallay, R.; Novak, P.; Kotz, R. Gas Evolution in Activated Carbon/Propylene Carbonate Based Double-Layer Capacitors. *Electrochem. Commun.* **2005**, *7*, 925–930.
35. Hahn, M.; Kotz, R.; Gallay, R.; Siggel, A. Pressure Evolution in Propylene Carbonate Based Electrochemical Double Layer Capacitors. *Electrochim. Acta* **2006**, *52*, 1709–1712.
36. Randles, J. E. B. Kinetics of Rapid Electrode Reactions. *Discuss. Faraday Soc.* **1947**, *1*, 11–19.
37. Zhu, H.; Zhao, G.-L.; Masarapu, C.; Young, D. P.; Wei, B. Q. Super Small Energy Gaps of Single-Walled Carbon Nanotube Strands. *Appl. Phys. Lett.* **2005**, *86*, 203107.
38. Wang, K. P.; Teng, H. Structural Feature and Double-Layer Capacitive Performance of Porous Carbon Powder Derived from Polyacrylonitrile-Based Carbon Fiber. *J. Electrochem. Soc.* **2007**, *154*, A993–A998.
39. Service, R. E. New 'Supercapacitor' Promises to Pack More Electrical Punch. *Science* **2006**, *313*, 902–905.